

Advanced Design of Block Shear Failure

Marta Kuříková^{1,*} , David Sekal¹ , František Wald¹  and Nadine Maier²

¹ Department of Steel and Timber Structures, Faculty of Civil Engineering, Czech Technical University in Prague, Thákurova 7, 166 29 Prague 6, Czech Republic; davidsekal@seznam.cz (D.S.); wald@fsv.cvut.cz (F.W.)

² Department of Civil, Geo and Environmental Engineering, Technical University of Munich, Arcisstraße 21, 80333 Munich, Germany; nadine.maier@tum.de

* Correspondence: marta.kurikova@fsv.cvut.cz

Abstract: This paper presents the behaviour and design procedure of bolted connections which tend to be sensitive to block shear failure. The finite element method is employed to examine the block shear failure. The research-oriented finite element method (RFEM) model is validated with the results of experimental tests. The validated model is used to verify the component-based FEM (CBFEM) model, which combines the analysis of internal forces by the finite element method and design of plates, bolts and welds by the component method (CM). The CBFEM model is verified by an analytical solution based on existing formulas. The method is developed for the design of generally loaded complicated joints, where the distribution of internal forces is complex. The resistance of the steel plates is controlled by limiting the plastic strain of plates and the strength of connectors, e.g., welds, bolts and anchor bolts. The design of plates at a post-critical stage is available to allow local buckling of slender plates. The prediction of the initial stiffness and the deformation capacity is included natively. Finally, a sensitivity study is prepared. The studied parameters include gusset plate thickness and pitch distance.



Citation: Kuříková, M.; Sekal, D.; Wald, F.; Maier, N. Advanced Design of Block Shear Failure. *Metals* **2021**, *11*, 1088. <https://doi.org/10.3390/met11071088>

Academic Editors:
Hussam Mahmoud and Ravi
Kiran Yellavajjala

Received: 29 April 2021
Accepted: 1 July 2021
Published: 8 July 2021

Publisher's Note: MDPI stays neutral with regard to jurisdictional claims in published maps and institutional affiliations.



Copyright: © 2021 by the authors. Licensee MDPI, Basel, Switzerland. This article is an open access article distributed under the terms and conditions of the Creative Commons Attribution (CC BY) license (<https://creativecommons.org/licenses/by/4.0/>).

Keywords: structural steel connections; bolted connections; finite element method; component-based FEM; block shear failure

1. Introduction

The block shear failure was first reported in 1978 in [1] for joints without optimal geometry from an internal forces point of view. The test results proved the potential failure mode of tearing out in the web of the beam. Several studies concerning the block shear failure were published in the last twenty years [2–7], predicting the block shear capacity as a combination of fracture on the tension and shear plane (see Figure 1). Block shear rupture is the potential failure mode for gusset plates, fin plates, coped beams, single/double angles and tee connections, where significant tension/shear forces are present.

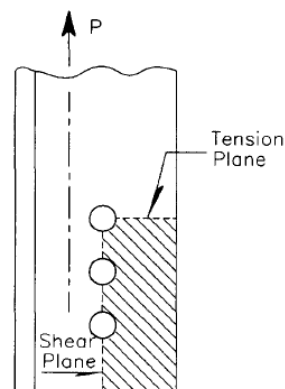


Figure 1. Typical block shear failure mechanism. Reproduced with permission from ref. [8], copyright (1995), Elsevier.

The analytical approaches of designing against block shear failure are described in standards. The design approaches are based on a simple assumption that the block shear capacity is the combination of the yielding along shear planes and rupture on the tensile plane. The analytical models used for verification in this study include currently valid Eurocode EN1993-1-8:2006 [9], US structural steel design code A360-16 [10], 2nd generation of Eurocode prEN1993-1-8 [11], which is planned to be issued after 2020, Canadian structural steel design standard CSA S16-09 [12] and analytical models proposed by Topkaya [5] and Driver [6]. The major advantage of these models is that they can be used in most cases and they are easy to apply, but no studies have dealt with complex loading, including substantial eccentricities and general block failure. Despite the existence of several design approaches to predict block shear capacity, the prediction of failure mode appears to have the same importance.

With the development of computational technology, it is possible to create advanced finite element models. These can be validated by experiments; therefore, the behaviour of numerical simulation is close to the physical test behaviour. Their main advantage is that once the appropriate finite element model is created, it is possible to carry a parametric study on it with minor modifications without the need for carrying out additional physical tests. However, making an accurate finite element model is laborious and, due to many variables, such as the definition of boundary conditions, meshing, etc., the results are not always representative. The finite element analysis of block shear failure has been developed since 2002, when numerical simulations were presented in [7]. The majority of the following numerical models covered the tensile fracture but not the shear rupture and development of a shear crack. The block shear failure, capturing the ductile fracture and combining both shear and tension failure, is presented in [4,13,14]. The prediction of the shear crack development in the bolted connection is presented by the appropriate failure criteria.

The approach, which combines the component method and finite element method, is called component-based FEM (CBFEM). As the name suggests, it combines aspects of the finite element method and component method to provide a satisfactory way of designing steel joints, while simultaneously complying with valid standards. Contrary to complex finite element simulations, it is commonly used for designing steel joints in practice. The CBFEM model is verified by the analytical and research-oriented FEM models comparing the block shear capacity in three levels of complexity.

2. Analytical Models for Resistance

2.1. Buckling

The buckling capacity and the compressive stress in the gusset plate may be determined according to Whitmore's effective width concept [15]. Thus, in design, the gusset plates are treated as rectangular members with a cross section $l_w \times t$, where l_w is the Whitmore's effective width l_w (see Figure 2). In fact, Whitmore defined the effective width as the distance perpendicular to the load, where 30° lines, which are projected from a first bolt row or the end of a weld, intersect with a line perpendicular to the member through a bottom bolt row or the second end of the weld.

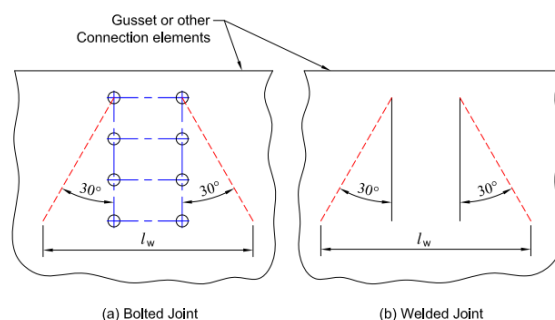


Figure 2. The Whitmore section [16].

A review of the design practice of connections with the block shear failure is published in [17]. The authors compared analytical models in different national standards (European, American, Canadian, Australian and Japanese) with gathered experimental results. They also separated the results into categories according to the connection type—gusset plate, coped beam, single angles and tees, double angles—and determined the safety ratio as: analytical model resistance/test results. Finally, analytical Equations (1) and (2) are given:

For angles and gusset plate:

$$P_u = A_{nt} \cdot \sigma_u + 0.6 \cdot \sigma_y \cdot A_{gv} \quad (1)$$

For coped beam webs:

$$P_u = 0.5 \cdot A_{nt} \cdot \sigma_u + 0.6 \cdot \sigma_y \cdot A_{gv} \quad (2)$$

where P_u is block tearing resistance, A_{nt} is net area subjected to tension, A_{gv} is gross area subjected to shear, σ_u is ultimate stress, σ_y is yield stress.

A numerical study using parametric finite element models validated on previous experiments is published in [5]. It was found that the stress on a shear plane is lower than the tension yield stress but higher than a shear stress $0.6F_y$. The so-called effective shear stress is given as a function of the connection length. The effective shear stress is decreased as the connection length increases.

The block shear capacity is:

$$R_n = \left(0.25 + 0.35 \frac{F_u}{F_y} - \frac{C_1}{2800} \right) F_y A_{gv} + F_u A_{nt} \quad (3)$$

where R_n is block tearing resistance, F_u is ultimate stress, F_y is yield stress, C_1 is connection length, A_{gv} is gross area subjected to shear, A_{nt} is net area subjected to tension.

The effect of in-plane/out-of-plane eccentricity is observed. The in-plane eccentricity decreases the resistance up to 15% and is mostly influenced by the connection length. It is also mentioned that for a connection length up to 150 mm, no reduction in capacity is needed. In the case of out-of-plane eccentricity, the difference between the connections without eccentricity was at most 5%. Due to these findings, it is concluded that the block shear capacity remains unaffected by out-of-plane eccentricity.

The database of block shear experiments, including gusset plate, angle, tee and coped beam tests, is collected in [6]. The block shear capacity depends on the type of connection with varying stress factors, R_t and R_v , and is determined as:

$$P_u = R_t A_{nt} F_u + R_v A_{gv} \left(\frac{F_y + F_u}{2\sqrt{3}} \right) \quad (4)$$

where P_u is block tearing resistance, R_t , R_v are equivalent stress factors for a unified equation, F_u is ultimate stress, F_y is yield stress, A_{gv} is gross area subjected to shear, A_{nt} is net area subjected to tension.

Equivalent stress factors vary from 0.3–1 according to the type of connection. The advantage of the formula is that it gives more realistic results than the codes do and that it is uniform for eccentric/concentric connections. On the other hand, additional factors are introduced, which goes against the idea of making the analytical models comprehensible and transparent. The influence of eccentric loading on block shear failure mode was studied in [18]. The suggested approach is to create simple interaction formulas related to the other ones used in codes for cross section analysis—the interaction of normal force, shear force and bending moment. In the end, there would be the simple Equation (5):

$$\left(\frac{N}{N_R} + \frac{M}{M_R} \right)^2 + \left(\frac{V}{V_R} \right)^2 \leq 1 \quad (5)$$

where N , M , V are actual section forces, N_R , M_R , V_R are individual resistances of the joint.

The rules presented in EN1993-1-8:2006 are separated into two categories—“symmetric group of bolts subjected to concentric loading” and “group of bolts subjected to eccentric loading”.

2.2. Concentric Loading

For concentric loading, the design block tearing resistance $V_{eff,1,Rd}$ is given by:

$$V_{eff,1,Rd} = \frac{f_u A_{nt}}{\gamma_{M2}} + \left(\frac{1}{\sqrt{3}} \right) f_y A_{nv} / \gamma_{M0} \quad (6)$$

where A_{nt} is net area subjected to tension, A_{nv} is net area subjected to shear, f_u is ultimate strength, f_y is yield stress.

Equation (6) represents the idea mentioned before, that the rupture on the tension plane occurs before the rupture on the shear plane that is caused by the steel having lower ductility in tension than in shear. Therefore, the ultimate strength for the tension plane and yield stress for the shear plane are used.

2.3. Eccentric Loading

For eccentric loading, the design block tearing resistance $V_{eff,2,Rd}$ is given by:

$$V_{eff,2,Rd} = 0.5 \cdot \frac{f_u A_{nt}}{\gamma_{M2}} + \left(\frac{1}{\sqrt{3}} \right) f_y A_{nv} / \gamma_{M0} \quad (7)$$

The 0.5 ratio represents non-uniform stress distribution due to eccentric loading, even though it seems to be, in most cases, a conservative solution and it does not consider the actual size of eccentricity. For A_{nt} , A_{nv} , A_{gv} , see Figure 3.

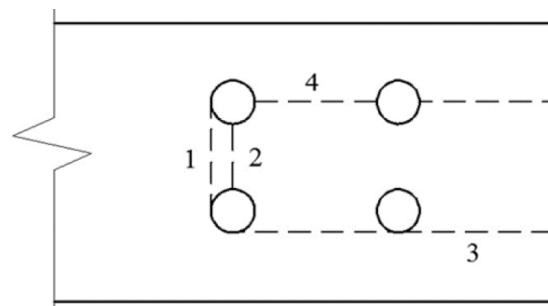


Figure 3. Failure planes during the block shear failure; 1—gross tensile plane A_{gt} ; 2—net tensile plane A_{nt} ; 3—gross shear plane A_{gv} ; 4—net shear plane A_{nv} .

The approach in AISC 360-16 of the American Institute of Steel Construction is less conservative than the current valid Eurocode formulas because it uses the ultimate strength for the shear resistance part. Nevertheless, the capacity is limited by the right side of Equation (8), which corresponds with the idea that when the yield stress is reached on the gross shear plane, the rupture appears on the tension plane. The factor U_{bs} reduces the tension plane resistance due to a non-uniform stress distribution in a same way as Eurocode does.

$$R_n = 0.6F_u A_{nv} + U_{bs} F_u A_{nt} \leq 0.6F_y A_{gv} + U_{bs} F_u A_{nt} \quad (8)$$

where R_n is block tearing resistance, A_{gv} is gross area subjected to shear, A_{nv} is net area subjected to shear, A_{nt} is net area subjected to tension, F_u is ultimate strength, F_y is yield strength, U_{bs} is 1.0 (for single-row beam end connections, welded or bolted angle connections, connections with gusset plates) or 0.5 (for multiple-row beam end connections).

The load resistance safety factor for the LRFD method is $\phi = 0.75$.

The prEN1993-1-8 has significantly changed its approach compared to the current code. The equations are still separated into two groups with respect to the position of an acting force.

2.4. Concentric Loading

$$V_{eff,1,Rd} = \left[A_{nt}f_u + \min\left(\frac{A_{gv} \cdot f_y}{\sqrt{3}}; \frac{A_{nv}f_u}{\sqrt{3}}\right) \right] / \gamma_{M2} \quad (9)$$

In contrast to the current Eurocode, the gross shear plane instead of the net shear plane is considered in Equation (9) which, according to [17], corresponds better with the experimental results. It also implements an idea similar to the AISC that there are two possible ways of block shear failure—either a rupture along the net shear plane followed by a rupture on a net tension plane (when the connection is short and wide), or the net tension rupture appears before the ultimate stress on a shear plane fully develops (in the case of long and narrow connections).

2.5. Eccentric Loading

$$V_{eff,2,Rd} = \left[0.5A_{nt}f_u + \min\left(\frac{A_{gv}f_y}{\sqrt{3}}; \frac{A_{nv}f_u}{\sqrt{3}}\right) \right] / \gamma_{M2} \quad (10)$$

The ratio 0.5 represents non-uniform stress distribution on a tension plane due to eccentric loading.

2.6. Research by Kim

Experimental studies on double-shear bolted connections fabricated with lean duplex stainless steel were conducted and the validation of the finite element analysis model was verified in the field of ultimate strength and fracture mode through a comparison with test results. Analysis strengths were compared with block shear predictions by the current design equations and suggested equations by previous researchers. A modified block shear strength equation was recommended considering the material properties of lean duplex stainless steel and the shear stress distribution in the critical shear section of block shear [19].

3. Experiments

3.1. Geometry

The experiments used in this work for validation were carried out and described in [7]. Two configurations of gusset plate bolted connections were tested—a long and narrow connection, T1, and a short and wide connection, T2—in order to propose a new analytical model for calculating block shear capacity. The test set-up is shown in Figure 4.

The geometries of tested specimens T1 and T2 are shown in Figure 5. The tested gusset plates were 6.6 mm thick, the bolts were $\frac{3}{4}$ inch (19 mm) and the bolt holes (19 mm) were match drilled so the bolts were in bearing from the beginning of the test. All the bolts were installed with a snug fit.

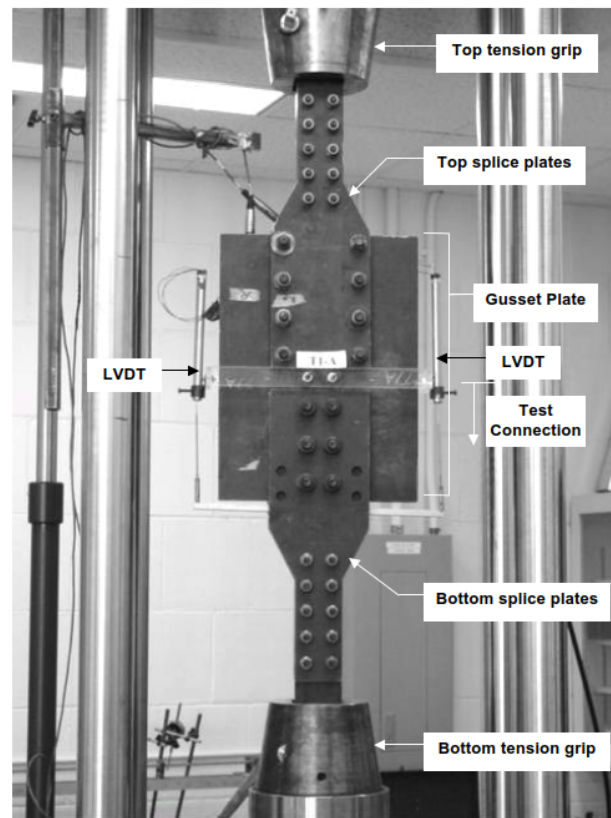


Figure 4. Test set-up for gusset plate connection [7].

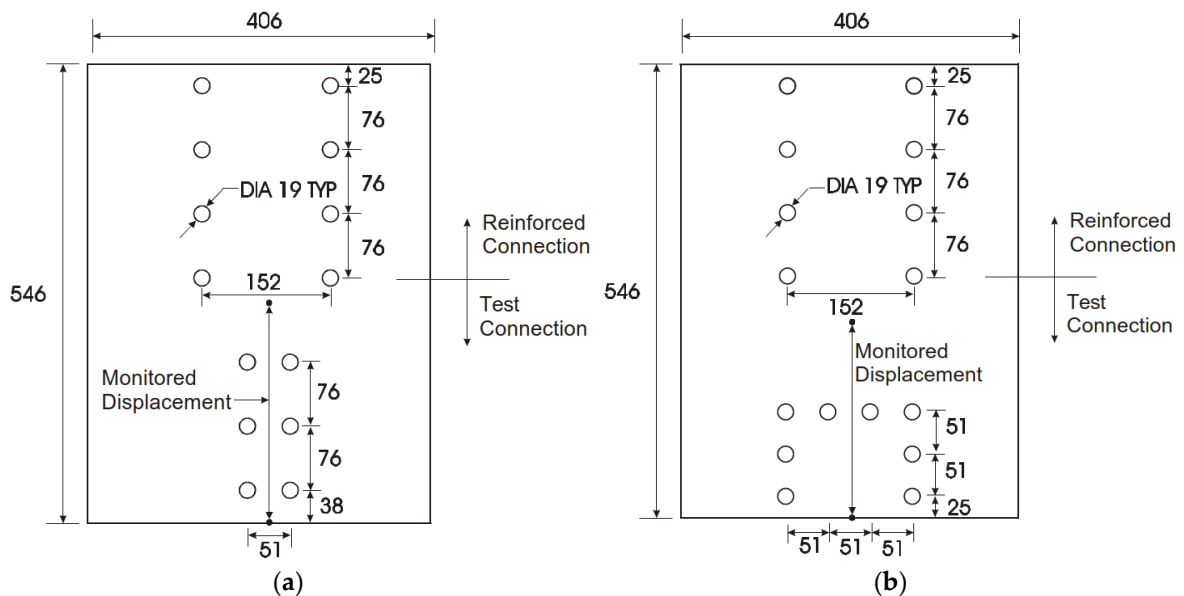


Figure 5. Tested gusset plate connections: (a) specimen T1 and (b) specimen T2 [7], dimensions in mm.

3.2. Material

The gusset plates and splice plates were grade 350 W steel. Since both specimens were made of the same steel sheet, mean values of F_y , F_u , ν and E applies for both (see Table 1). As for the description of plastic hardening, a multilinear function (true stress–true strain) was used. The nonlinear material behaviour was described in [7] and derived from coupon tensions tests. The nonlinear part starts at a yield point, where the elastic part of the stress

versus strain curve ends (see Figure 6). Up to that point, there is a linear function that has a slope coefficient equal to E .

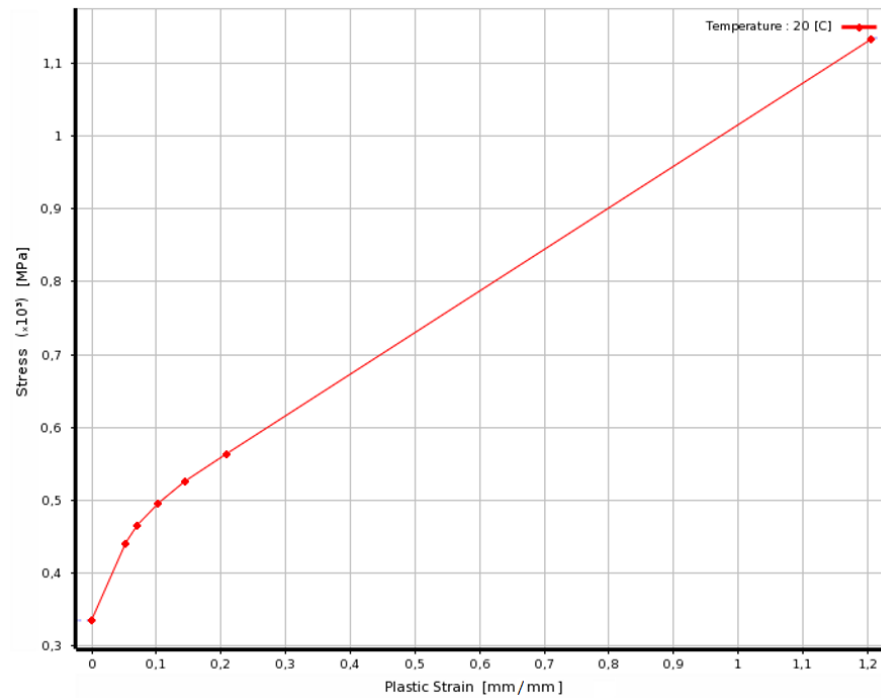


Figure 6. Stress vs. strain curve of gusset plate material, ANSYS interface.

Table 1. Material properties, mean value.

Plate Properties:	
Modulus of elasticity— E (MPa)	197,553
Static yield stress— F_y (MPa)	336
Static ultimate stress— F_u (MPa)	450
Poisson’s ratio— ν (-)	0.3
Bolts A325:	
Modulus of elasticity— E (MPa)	200,000
Static yield stress— F_y (MPa)	660
Static ultimate stress— F_u (MPa)	830

3.3. Experimental Results

The specimens at the end of testing are shown in Figure 7. Each of the specimens was tested to failure on the shear planes.



Figure 7. (a) Specimen T1 and (b) specimen T2 at the end of testing [7].

4. Research-Oriented Finite Element Model

4.1. Model Geometry

The general finite element (FE) program ANSYS was employed in the numerical simulations. Since the deformation during the test was measured symmetrically at the beginning and at the end of the connection, half of the specimen was modelled. The reduced model geometries can be seen in Figure 8.

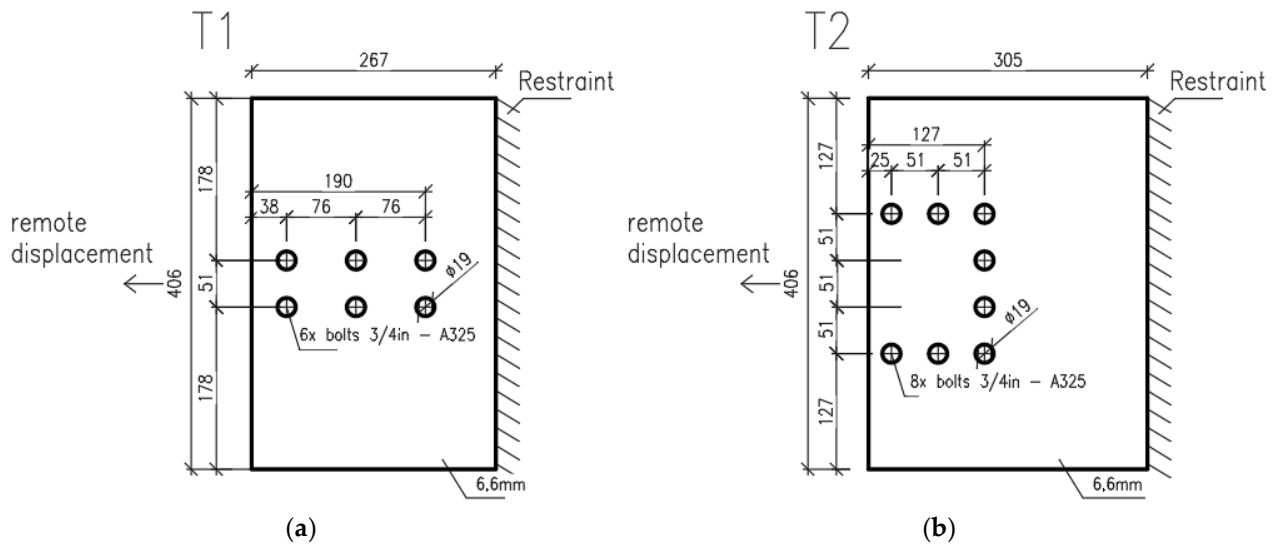


Figure 8. Simplified geometries used for FEM simulations: (a) specimen T1 and (b) specimen T2 [7], dimensions in mm.

4.2. Loading and Mesh

The splices were significantly thicker and therefore much more rigid than the inspected gusset plates. The splices were not modelled, so no interface between the plates was applied. It was assumed that all the bolts moved together in a rigid frame defined by the initial pitches and gauge distances. The loading process was represented by a remote displacement that matched the test procedure. The remote displacement was applied in the bolt hole where the bolt shank was in contact. The remote displacement was applied on the nodes on half (since the bolts were match drilled) of each bolt hole in the chosen direction.

Bolts were simplified as only bearing displacements on the half-circle of the bolt hole (see Figure 9). The deformation was applied in the bolt hole where the bolt shank was in contact. The displacements in all holes were coupled together.

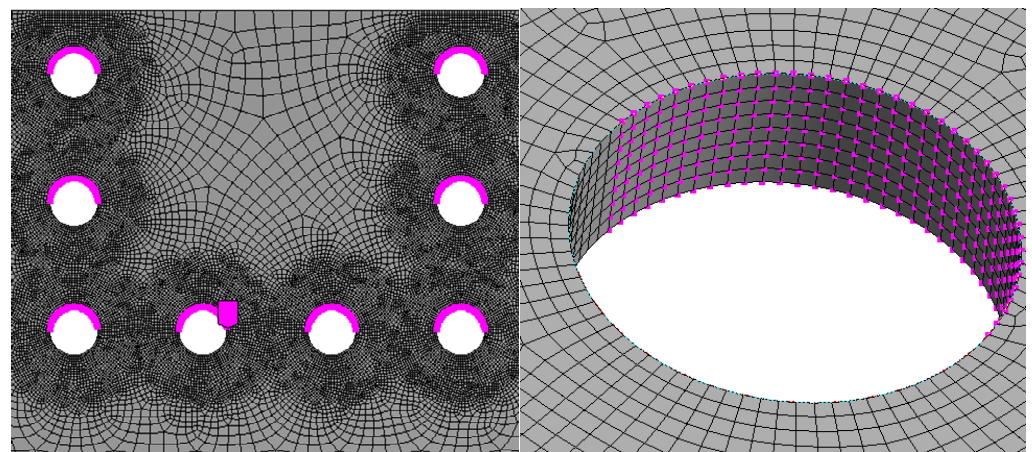


Figure 9. Mesh refinement around bolt holes in RFEM model.

Hexahedron-dominant mesh was used with $1 \times 1 \text{ mm}^2$ refinement in areas where a high gradient was expected—locally, around the bolt holes with a radially structured grid. The analysis was material and geometric nonlinear. Large deformation analysis was used and the Newton–Raphson method of equations was chosen for solving systems. The number of loading steps was set to 50, the convergence criteria for tolerance to 1.0% and the maximum number of iterations to 50. Loading was applied through displacement increments, which better reflected the experimental conditions. The analysis stopped at a certain limit of displacement, when the tension fracture appeared.

4.3. Validation

The numerical solution, in this case the RFEM model, was validated on the experimental data. The load–deflection behaviour of the tested specimens was compared and the results for the specimen T1 are summarised in Table 2 and for the specimen T2 in Table 3. The load–deflection curves comparing the experimental and numerical results are shown in Figures 10 and 11. The compared parameters include failure mode, initial stiffness $N_{j,ini}$, peak load F_{peak} , resistance at 2 mm deformation F_{2mm} , resistance at 5% plastic strain $F_{0.05}$ and serviceability limit state resistance at 2/3 of test ultimate deformation $F_{2/3}$.

Table 2. Results of validation, T1.

T1 Specimen		Values		Experiment/RFEM Ratio (-)
Compared Parameters	Units	Experiment	RFEM	
$N_{j,ini}$	(MN/m)	1717.7	2153.4	0.80
F_{peak}	(kN)	691.2	698.1	0.99
F_{2mm}	(kN)	586.2	580.1	1.01
$F_{0.05}$	(kN)	N/A	486.3	N/A
$F_{2/3}$	(kN)	663.0	654.5	1.01

Table 3. Results of validation, T2.

T2 Specimen		Values		Experiment/RFEM Ratio (-)
Compared Parameters	Units	Experiment	RFEM	
$N_{j,ini}$	(MN/m)	1846.4	1773.1	1.04
F_{peak}	(kN)	756.0	742.9	1.02
F_{2mm}	(kN)	639.9	643.3	0.99
$F_{0.05}$	(kN)	N/A	421.0	N/A
$F_{2/3}$	(kN)	727.0	726.5	1.00

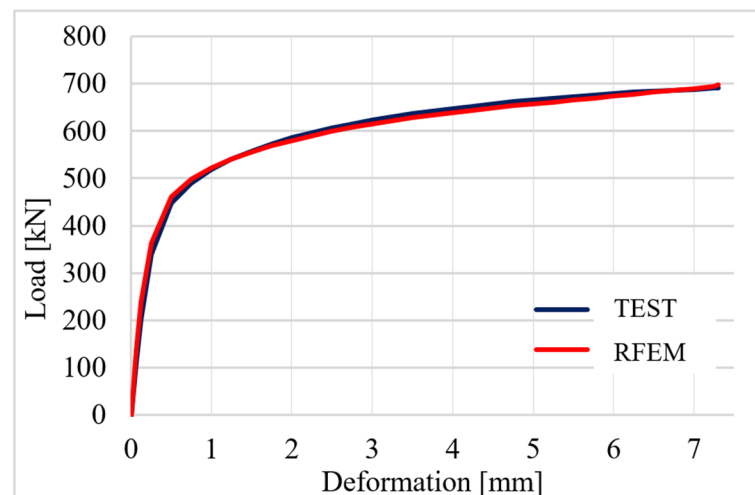


Figure 10. Load vs. deflection curve, RFEM and experimental curves of specimen T1.

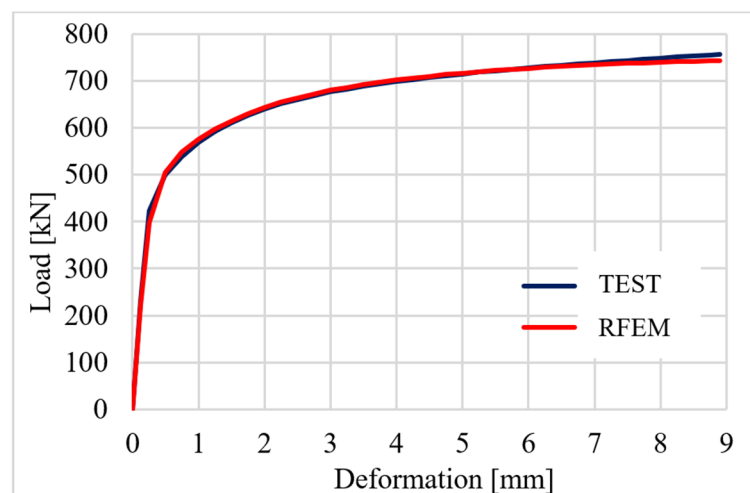


Figure 11. Load vs. deflection curve, RFEM and experimental curves of specimen T2.

Despite some differences between numerical simulation and physical tests, there is a good rate of compliance in tested parameters. The maximal difference between the compared values is 20% in the case of initial stiffness of the T1 model (see Table 2). For initial stiffness, the higher rate of difference is acceptable because the value is dependent on many factors, for example, the mesh size around the bolt holes or the initial contact area influencing the bearing of bolts in experimental tests. However, besides this one value, the other compared parameters vary from 0–4% so the models can be used for the verification of design-oriented models.

Additionally, it is worth noting that in a deformed numerical model, signs typical of block shear failure mechanisms could be observed, such as necking on a tension plane and yielding on the outer plane of bolt holes (see Figure 12).

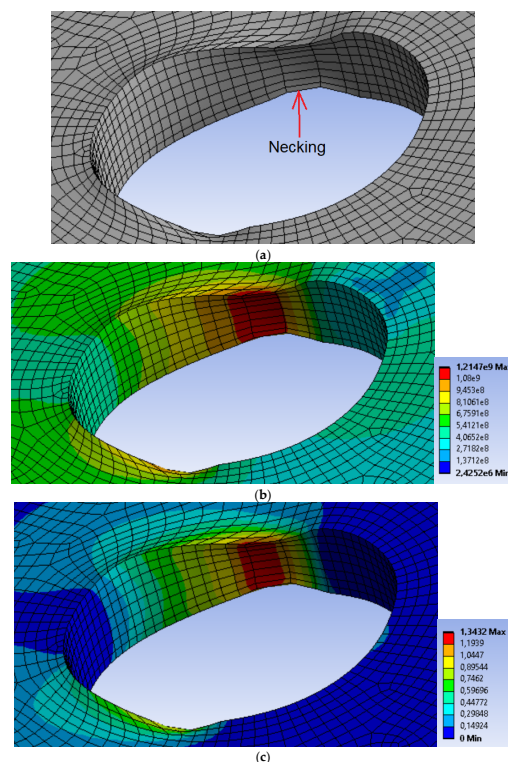


Figure 12. Deformed bolt hole of specimen T2 at tension fracture, (a) necking on a tension plane, (b) equivalent (von Mises) stress in Pa, (c) equivalent plastic strain in m/m.

5. Design-Oriented Finite Element Analysis

5.1. Model

Design-oriented finite element analysis was carried out with the software IDEA StatiCa. The software combines the finite element method with the component method and offers an alternative to conventional analytical models and the laborious component method. Contrary to RFEM, IDEA software uses 2D shell elements for plates, whereas fasteners (welds, bolts, contacts, etc.) are represented by components with pre-defined properties based on experimental findings.

The elastoplastic material with strain hardening was modelled according to EN 1993-1-5:2006. The material behaviour was based on the von Mises yield criterion. It was assumed to be elastic before reaching the yield strength f_y . The ultimate limit state criterion for regions not susceptible to buckling is reaching a limiting value of the principal membrane strain. A value of 5% is recommended.

Plates were modelled by 4-node quadrangle shell elements. Each node had 6 degrees of freedom. The deformations of the element consisted of membrane and flexural contributions. Rotations perpendicular to the element were included by a full 3D formulation of the element. The formulation of the membrane behaviour was based on the study by Ibrahim-begovic [20]. The deformation of the nodes was represented by a bilinear stress–strain diagram. A quadratic basis function was considered along the element edges. The basis function represented the rotation perpendicular to the element. The flexural deformation was based on the Mindlin hypothesis, considering shear deformation, specifically on the MITC4 element [21]. A normal axis rotation of the plate was described by bilinear functions. The shear deformation was constant along the element edge. The resulting internal forces in the nodes and the element stiffness matrix were calculated by integrating over four Gauss points. The plastic behaviour was solved in each integration point. Every point was split into 5 integration points along the thickness of the element (Gauss–Lobatto integration). The nonlinear elastic-plastic stage of material was analysed in each layer based on the known strains.

Contact elements were used to transmit the pressure forces between plates. The standard penalty method was used for modelling the contact between the plates. The penalty stiffness was considered between the node and the opposite plate, when penetration into the opposite contact surface was detected. The penalty stiffness was controlled by a heuristic algorithm during the nonlinear calculation to ensure the convergence of the iteration. The solver detected the contact points and created an interpolation link between the penetrating nodes and the nodes on the opposite plate. The advantage of the penalty method is the automatic assembly of the model. The contact between the plates has a major impact on the redistribution of the forces in the connection [22].

Bolts were divided into three sub-components, which simulated the tensile behaviour of the bolt shank, the contact between the plate and the bolt head, nut or washer and the contact between the bolt shank and the plate. The bolt shank was modelled as a nonlinear spring, which did not transfer pressure forces. The pressure was transmitted by contact elements between the connected plates. The second sub-component transmitted tensile forces from the bolt to the plate. An interpolation link (a multi-point constraint) was inserted between the bolt shank and the flange nodes. The third sub-component ensured the shear transmission. The shear forces were transferred on the shank–hole face. This was modelled with the aid of contact elements between the node of the bolt shank and the nodes of the edges of the opening. The bolt shank transferred compression forces in the bolt hole. The stiffness of the shell elements around the opening was designed in such a way that a corresponding bearing strength was achieved when the plastic material of the plate was used. More about the design approach of a T-stub component by the component-based finite element method (CBFEM) is in [23].

Two CBFEM models with geometries and materials corresponding to the physical tests described in Section 2 were created. The models are shown in Figure 13.

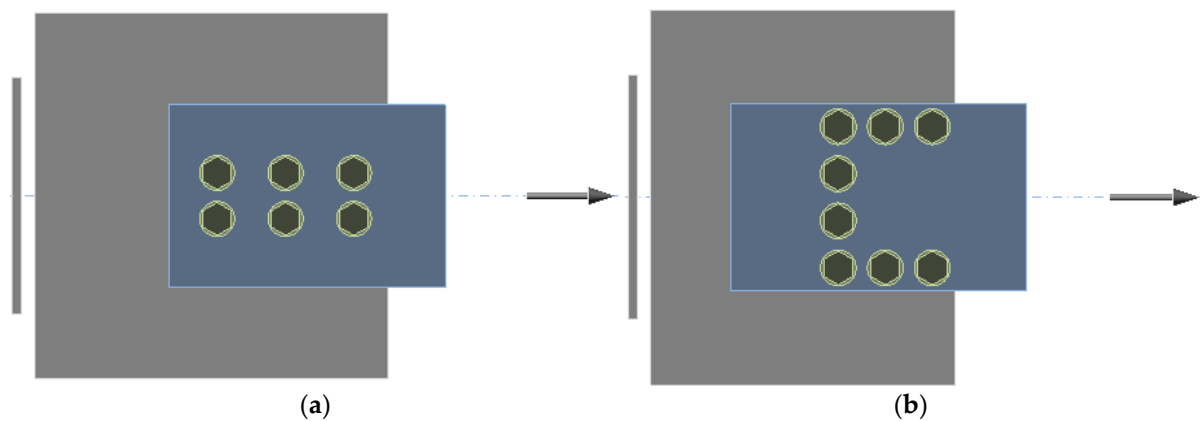


Figure 13. CBFEM model of (a) specimen T1 and (b) specimen T2.

The default configuration AISC 360-16 was used, material factors were equal to 1.0 and the finite element size was set to vary from 5 to 10 mm. The ultimate load for CBFEM models was assumed to appear when the plastic strain reached 5%.

5.2. Verification

The comparison of RFEM, CBFEM and analytical models is shown in Figures 14 and 15. The most conservative is the model in EN1993-1-8:2006 because, unlike other models, it uses the net shear plane in combination with yield stress, while yielding in the gross shear plane is observed in experiments and numerical models. In the next generation of Eurocodes (prEN1993-1-8), the formula for block shear resistance will be changed. The stiffness of the CBFEM model is lower compared to the RFEM model. The RFEM model disregards any slip, but in CBFEM, the shear model of bolts is according to a standard approximated with the assumption of regular bolt holes.

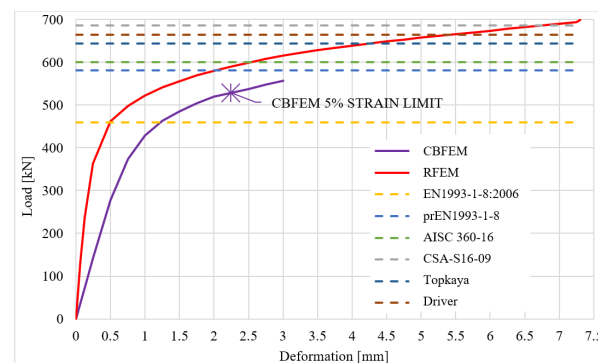


Figure 14. Comparison of RFEM, CBFEM and analytical models for specimen T1.

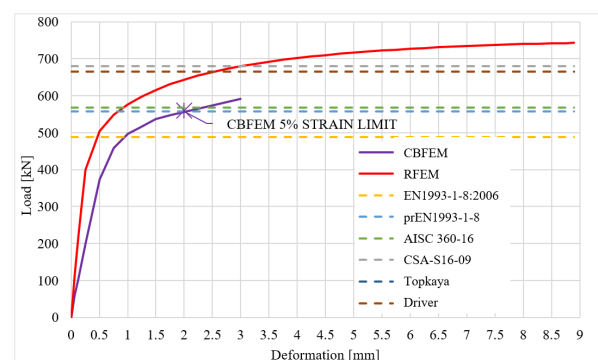


Figure 15. Comparison of RFEM, CBFEM and analytical models for specimen T2.

The results show that the CBFEM model is conservative compared to analytical models, except the current valid EN1993-1-8:2006. There is also a very high rate of compliance with the upcoming prEN1993-1-8 (90% and 99%) and with AISC 360-16 (87% and 98%). As was mentioned before, the EN1993-1-8:2006 does not consider two possible modes of block tearing progress and, unlike other models, it uses the net shear plane in combination with yield stress.

The correlation between design-oriented and research-oriented models is very good and the CBFEM results are on the safe side, except the $F_{0.05}$ value. The comparison of CBFEM and RFEM models are in Table 4 for specimen T1 and in Table 5 for specimen T2. For both CBFEM models, the initial stiffness $N_{j,ini}$ seems overly conservative when compared to the RFEM model, even though the higher rate of difference is acceptable in the case of initial stiffness. This may be caused by the different meshing of each model, more advanced material description in the RFEM model (plastic hardening), component representation of bolts in the case of CBFEM instead of infinitely rigid remote displacement used in RFEM and deformation of splice plates in the CBFEM model.

Table 4. Comparison of CBFEM and RFEM models for specimen T1.

T1 Specimen		Values		CBFEM/RFEM Ratio (-)
Compared Parameters	Units	RFEM	CBFEM	
$N_{j,ini}$	(MN/m)	2153.4	594.3	0.28
F_{peak}	(kN)	698.1	523.0	0.75
F_{2mm}	(kN)	580.1	519.7	0.90
$F_{0.05}$	(kN)	486.3	523.0	1.08
$F_{2/3}$	(kN)	654.5	519.7	0.79

Table 5. Comparison of CBFEM and RFEM models for specimen T2.

T2 Specimen		Values		CBFEM/RFEM Ratio (-)
Compared Parameters	Units	RFEM	CBFEM	
$N_{j,ini}$	(MN/m)	1773.1	932.8	0.53
F_{peak}	(kN)	742.9	554.4	0.75
F_{2mm}	(kN)	643.3	556.3	0.86
$F_{0.05}$	(kN)	421.0	554.4	1.32
$F_{2/3}$	(kN)	726.5	556.2	0.77

The distinction between $F_{0.05}$ values is probably caused by the fact that the strain is a local characteristic and it is highly dependent on the mesh element size. The difference between mesh density of the research-oriented model and the design-oriented model is significant and causes the increased plastic strain in RFEM.

6. Sensitivity Study

The CBFEM model T1 was used to study the influence of input parameters on the resistance of the joint. The tested parameters were the pitch distance and plate thickness. The output value subjected to comparison was the ultimate strength of the joint, which was compared to the results obtained by different design standards.

The CBFEM model ultimate resistances were calculated according to AISC 360-16 standard with the LRFD method. The ultimate resistance for the CBFEM model was assumed to appear when the strain reached 5%. The CBFEM results were plotted together with the analytical model results of recent/upcoming codes—EN1993-1-8:2006, AISC 360-16, prEN1993-1-8.

Specimen T1 was used to study the influence of the bolt pitch (Figure 16) and the plate thickness (Figure 17) on the block shear resistance. The bolt pitch was successively set to 56, 66, 76, 86, 96 and 106 mm. The study was carried out on 6 different plate thicknesses: 4.6; 5.6; 6.6; 7.6; 8.6 and 9.6 mm. The models provide expected results and show the increase in

block shear resistance with increased parameters in the case of symmetrical loading. The EN1993-1-8:2006 is the most conservative, followed by CBFEM, prEN1993-1-8 and AISC 360-16.

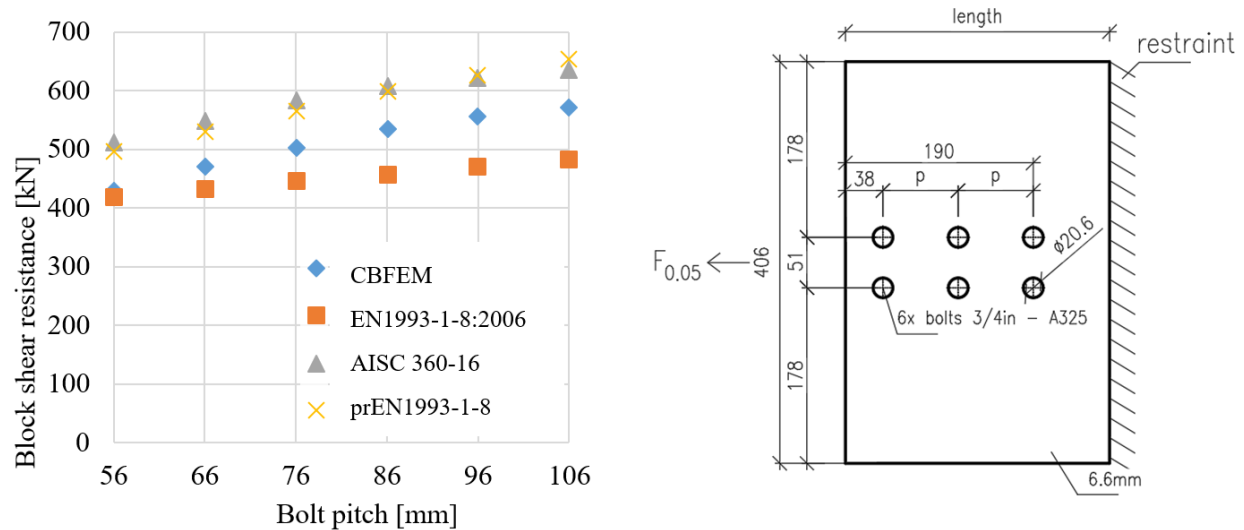


Figure 16. Sensitivity study of block shear resistance for bolt pitch, dimensions in mm.

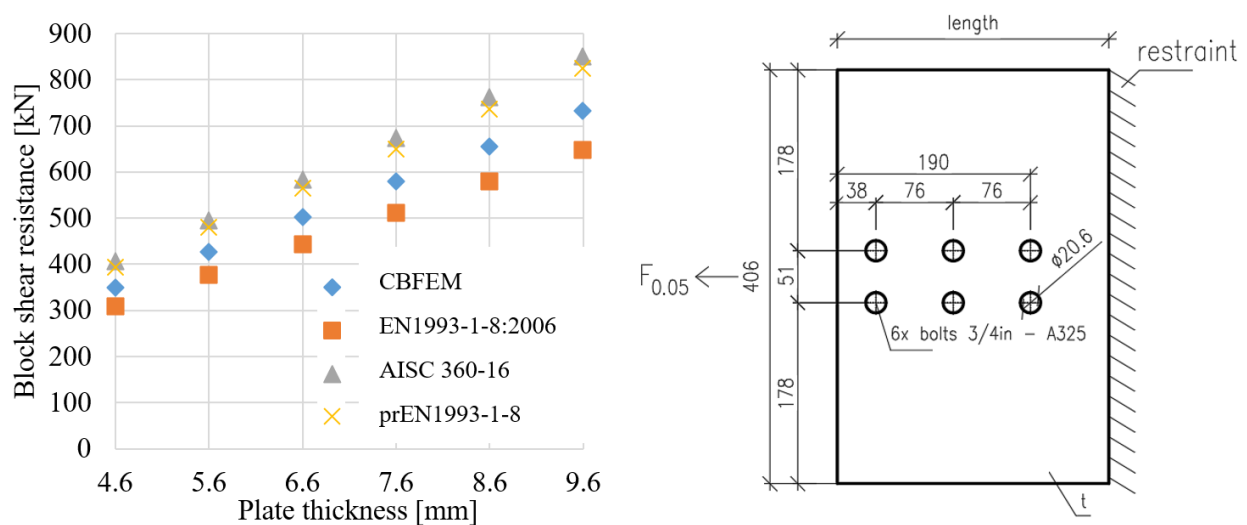


Figure 17. Sensitivity study of block shear resistance for plate thickness, dimensions in mm.

The steel grade S235 and bolts M22 grade 10.9 were used in the sensitivity study of eccentrically loaded bolted connection. Material safety factors were set to one. The geometry of the joint is shown in Figure 18. The load deflection curves of CBFEM and analytical models are shown in Figure 19. The analytical models used in codes use a constant reduction factor regardless of the magnitude of the eccentricity. It was claimed in [5,6] that the effect of in-plane eccentricity is not crucial for the total resistance, up to a 10% reduction. The reduction in resistance is significantly higher for analytical models used in the current codes. The results of the CBFEM model lie between the models presented in [5,6] and those used in codes. In contrast to analytical models where a constant reduction in resistance is used, CBFEM models employ finite element analysis for the calculations which may be advantageous in covering the actual size of the eccentricity.

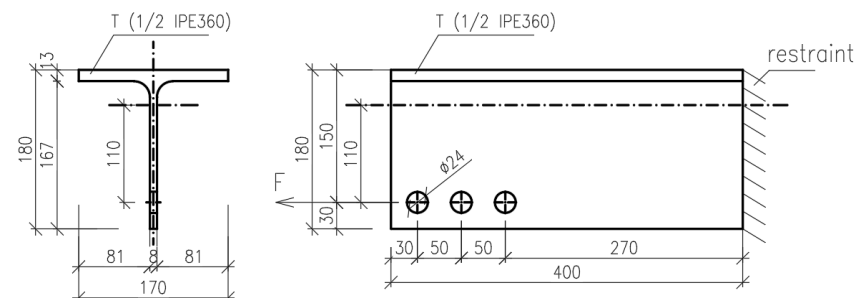


Figure 18. Geometry of the eccentrically loaded bolted connection used for FEM simulation, dimensions in mm.

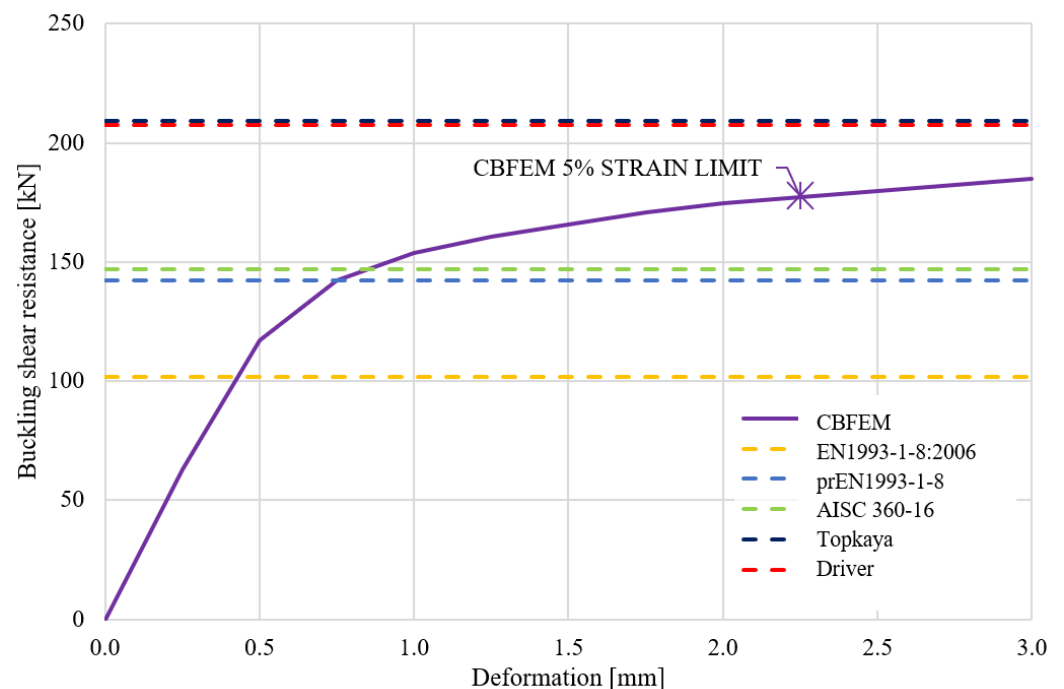


Figure 19. Load–deflection curve of eccentric bolted connection.

CBFEM models were created and compared to analytical models. If the currently valid EN 1993-1-8:2006 is excluded from the comparison, in the case of concentric connections, the CBFEM models have a good rate of compliance with analytical models and, except for one case, they are on the safe side. Models calculated according to prEN1993-1-8:2020 and AISC 360-16 were used. The study was carried out for four different pitch distances $p = 56; 66; 76$ and 86 mm, and six different plate thicknesses $t = 4.6; 5.6; 6.6; 7.6; 8.6$ and 9.6 mm. The bolt grade was A325 and 10.9 according to the relevant design standards. The results of sensitivity studies for concentric and eccentric bolted connections are summarised and shown in Figure 20. The CBFEM method is conservative for concentric connections and predicts up to 13.3% lower resistance. The validated models for eccentric connections predict up to 21% higher resistance.

The CBFEM model uses a bilinear material diagram with negligible strain hardening. On the other hand, the analytical models use a combination of yield and ultimate strengths in their formulas. The CBFEM model provides lower block shear resistances compared to the analytical models if a steel grade with a high ratio of ultimate to yield strength is used. Mesh refinement slightly decreases the block shear resistance; however, the mesh size near bolt holes is fixed.

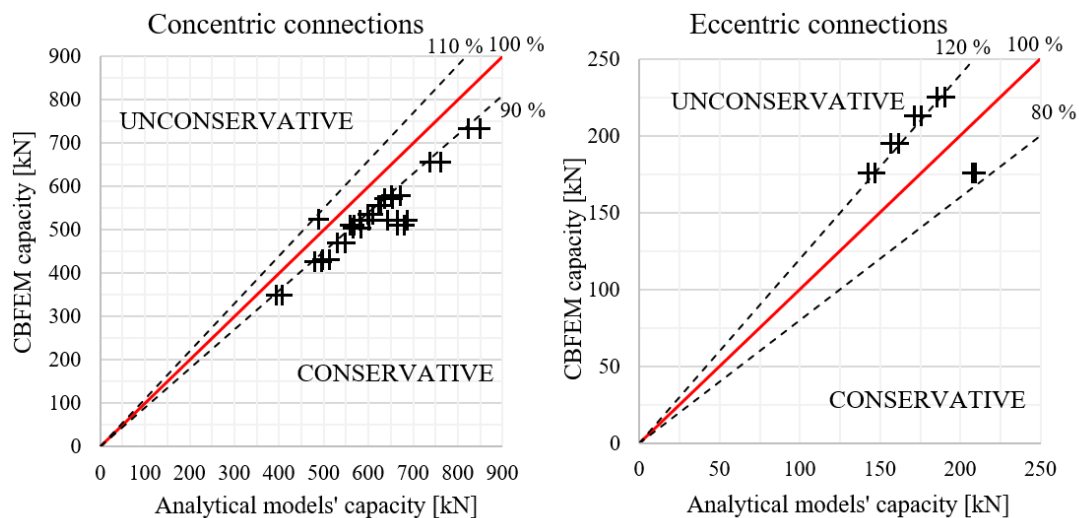


Figure 20. Comparison between analytical models and CBFEM.

7. Conclusions

In this study, research-oriented and design-oriented numerical models on block shear in gusset plate bolted connections were analysed. The experimental data published by [7] served for validations of the research-oriented models. The validated model correlated well with the experimental data in terms of failure modes, initial stiffness and resistance. A component-based finite element model was created and verified on the RFEM model. Load–deflection curves were plotted and the block shear resistance and initial stiffness were compared. The verification confirmed the CBFEM model as an appropriate numerical approach to predict the behaviour of gusset plate connections subjected to block shear failure and offers safe standard approval of resistance. The CBFEM is unconservative compared to all available codes in the case of eccentric connections. However, compared to models by Topkaya and Driver, it is conservative. There is a possibility to extend the study and continue the research in this way. The resistance of the gusset plate connections with various bolt pitches and plate thicknesses was explored and summarised for concentric and eccentric assemblies.

Author Contributions: Conceptualization, M.K.; methodology, F.W. and M.K.; software, D.S.; validation, D.S.; formal analysis, M.K.; investigation, D.S.; resources, D.S.; data curation, D.S.; writing—original draft preparation, D.S., F.W. and M.K.; writing—review and editing, M.K. and F.W.; visualization, D.S. and M.K.; supervision, N.M. and F.W.; project administration, F.W.; funding acquisition, F.W. All authors have read and agreed to the published version of the manuscript.

Funding: The work was prepared under the R&D project MERLION III supported by Technology Agency of the Czech Republic, project No. FW01010392.

Data Availability Statement: The data published in this article are taken from the diploma thesis, which is available at: <https://dspace.cvut.cz/handle/10467/81199>, accessed on 8 July 2021.

Conflicts of Interest: The authors declare no conflict of interest.

References

1. Birkemoe, P.C.; Gilmore, M.I. Behavior of Bearing Critical Double-Angle Beam Connections. *Eng. J.* **1978**, *15*, 109–115.
2. Clements, D.A.; Teh, L.H. Active Shear Planes of Bolted Connections Failing in Block Shear. *J. Struct. Eng.* **2013**, *139*. [[CrossRef](#)]
3. Teh, L.H.; Uz, M.E. Block shear failure planes of bolted connections—Direct experimental verifications. *J. Constr. Steel Res.* **2015**, *111*, 70–74. [[CrossRef](#)]
4. Wen, H.; Mahmoud, H. Simulation of block shear fracture in bolted connections. *J. Constr. Steel Res.* **2017**, *134*, 1–16. [[CrossRef](#)]
5. Topkaya, C.A. Finite Element Parametric Study on Block Shear Failure of Steel Tension Members. *J. Constr. Steel Res.* **2004**, *60*, 1615–1635. [[CrossRef](#)]

6. Driver, R.G.; Grondin, G.Y.; Kulak, G.L. Unified block shear equation for achieving consistent reliability. *J. Constr. Steel Res.* **2006**, *62*, 210–222. [[CrossRef](#)]
7. Grondin, G.Y.; Huns, B.B.S.; Driver, R.G. *Block Shear Behaviour of Bolted Gusset Plates*; Structural engineering report No. 248; University of Alberta: Edmonton, AB, Canada, 2002.
8. Cunningham, T.J.; Orbison, J.G.; Ziemian, R.D. Assessment of American block shear load capacity predictions. *J. Constr. Steel Res.* **1995**, *35*, 323–338. [[CrossRef](#)]
9. CEN. *Eurocode 3: Design of Steel Structures—Part 1–8: Design of Joints*; EN1993-1-8; CEN: Brussels, Belgium, 2006.
10. American Institute of Steel Construction. *Specification for Structural Steel Buildings*; ANSI/AISC 360-16; American Institute of Steel Construction: Chicago, IL, USA, 2016.
11. CEN. *Eurocode 3: Design of Steel Structures—Part 1–8: Design of Joints*; prEN1993-1-8; Final draft; CEN: Brussels, Belgium, 2020.
12. Canadian Standard Association. *Design of Steel Structures, CSA S16-09*; Canadian Standard Association: Mississauga, ON, Canada, 2009.
13. Kim, T.; Kuwamura, H. Finite element modelling of bolted connections in thin walled stainless steel plates under static shear. *Thin Walled Struct.* **2007**, *45*, 407–421. [[CrossRef](#)]
14. Adewole, J.J.; Joy, O.O. Finite-element block shear failure deformation-to-fracture failure analysis. *Can. J. Civ. Eng.* **2020**, *47*, 418–427. [[CrossRef](#)]
15. Whitmore, R.E. *Experimental Investigation of Stresses in Gusset Plates*; Bulletin No. 16; Engineering Experiment Station, University of Tennessee: Knoxville, TN, USA, 1952.
16. Thornton, W.A.; Carlo, L. The Whitmore Section: How to use the Whitmore method for tension and compression strength checks. In *Modern Steel Construction*; American Institute of Steel Construction: Chicago, IL, USA, 20 July 2011; pp. 52–56.
17. Kulak, G.L.; Grondin, G.Y. Block Shear Failure in Steel Members—A Review of Design Practice. *Eng. J.* **2001**, *38*, 329–339.
18. Jönsson, J. Block failure in connections—including effects of eccentric loads. In Proceedings of the 7th European Conference on Steel and Composite Structures (EUROSTEEL 2014), Napoli, Italy, 10–12 September 2014.
19. Kim, T.; Hong, S.; Hwang, B.; Kim, J. Block shear capacity in cold-formed lean duplex stainless steel double-shear bolted connections. *Thin Walled Struct.* **2021**, *161*, 107520. [[CrossRef](#)]
20. Ibrahimbegovic, A.; Taylor, R.L.; Wilson, E.L. A robust quadrilateral membrane finite element with drilling degrees of freedom. *Int. J. Numer. Methods Eng.* **1990**, *30*, 445–457. [[CrossRef](#)]
21. Dvorkin, E.N.; Bathe, K.J. A continuum mechanics based four-node shell element for general non-linear analysis. *Eng. Comput.* **1984**, *1*, 77–88. [[CrossRef](#)]
22. Wald, F.; Vild, M.; Kuříková, M.; Kabeláč, J.; Sekal, D.; Maier, N.; Da Silva Seco, L.; Couchaux, M. Finite-Element-Bemessung von Stahlverbindungen basierend auf der Komponentenmethode. *Stahlbau* **2020**, *89*, 482–495. [[CrossRef](#)]
23. Gödrich, L.; Wald, F.; Kabeláč, J.; Kuříková, M. Design finite element model of a bolted T-stub connection component. *J. Constr. Steel Res.* **2019**, *157*, 198–206. [[CrossRef](#)]